Thermochimica Acta 608 (2015) 49–58

Contents lists available at ScienceDirect

Thermochimica Acta

journal homepage: www.elsevier.com/locate/tca

Thermodynamic modeling of the Co–Hf system supported by key experiments and first-principles calculations

Xingxu Lu [a,b], Shuhong Liu [b,d,*], Kaiming Cheng [b], Ying Tang [b], Pengfei Ou [a,b], Philip Nash [c], Bo Sundman [e], Yong Du [b,d], Feng Zheng [a]

[a] School of Materials Science and Engineering, Central South University, Changsha, Hunan 410083, China
[b] State Key Laboratory of Powder Metallurgy, Central South University, Changsha, Hunan 410083, China
[c] Thermal Processing Technology Center, Illinois Institute of Technology (IIT), 10 West 32nd Street, Chicago, IL 60616, USA
[d] Sino-German Cooperation Group "Microstructure in Al alloys", Central South University, Changsha, Hunan 410083, China
[e] INSTN, CEA Saclay, 91191 Gif-Sur-Yvette Cedex, France

ARTICLE INFO

Article history:
Received 24 January 2015
Received in revised form 2 April 2015
Accepted 5 April 2015
Available online 7 April 2015

Keywords:
Co–Hf system
Cobalt-based alloys
Amorphous alloys
Drop calorimetry
First-principles calculations
CALPHAD

ABSTRACT

Phase equilibria and thermodynamic properties of the Co–Hf system were investigated via calorimetric measurements, first-principles calculations and thermodynamic modeling. Heat contents of Co_2Hf and $CoHf_2$ were measured by drop calorimetry from 300 to 1200 °C. The enthalpy of formation for $Co_{23}Hf_6$ at 0 K was computed via first-principles calculations. Based on the experimental measurements and first-principles calculations from the present work and the literature, the Co–Hf system was assessed by means of CALPHAD (CALculation of PHAse Diagram) approach. The excess Gibbs energy of solution phases was modeled with Redlich–Kister polynomial. Sublattice models were employed to describe the homogeneity ranges of Co_2Hf, CoHf and $CoHf_2$. The order–disorder transition between B2 (CoHf) and A2 (βHf) phases was taken into account in the current optimization. Using the optimized parameters, glass forming range (GFR) of the Co–Hf amorphous alloys was predicted to be 15–75 at.% Hf, which is in satisfactory agreement with the experimental observation.

1. Introduction

Cobalt-based alloys are known for the unique combinations of properties, such as high temperature creep and fatigue strength as well as good resistance to aggressive corrosion and various forms of wear [1]. Recent studies have shown that small additions of Hf into Co–Al–W ternary system can stabilize the γ′-Co_3(Al,W) phase, making it possible to develop a new class of cobalt-based alloys with a greater high-temperature strength than that of the conventional nickel-based superalloys [2–4]. Meanwhile, the Co–Hf binary alloys were also reported to be able to form metallic glass over a wide range of composition, and have been investigated as a promising bulk metallic glass (BMG) system by several authors [5–10]. Therefore, in order to control the microstructures in multi-component cobalt-based superalloys and to develop new classes of bulk amorphous materials, knowledge of accurate thermodynamic description of the Co–Hf binary system is necessary.

The Co–Hf phase diagram was critically assessed by Ishida and Nishizawa [11] based on the previous experimental investigations [12–14], and their work was accepted by Okamoto [15] during his review on the system. With limited experimental information, Bratberg and Jansson [16] performed a simplified thermodynamic assessment for the Co–Hf system. However, the calculated phase diagram deviates greatly from the assessed work by Ishida and Nishizawa [11], as shown in Fig. 1. Recently, the Co–Hf binary phase diagram was systematically investigated by the present authors [17], and the phase equilibria were revised based on the reliable experimental observations. On the other hand, thermodynamic information for the Co–Hf binary compounds is relatively limited, making it difficult to perform accurate thermodynamic modeling for the system.

Therefore, the objective of the present work is to develop a set of self-consistent thermodynamic parameters for the Co–Hf system via a hybrid approach of calorimetric experiments, first-principles calculations and CALPHAD (calculation of phase

* Corresponding author at: State Key Lab of Powder Metallurgy, Central South University, Changsha, Hunan 410083, China. Tel.: +86 731 888 77300; fax: +86 731 887 10855.
E-mail addresses: shhliu@csu.edu.cn, http://www.imdpm.net/LiuSH.htm (S. Liu).

http://dx.doi.org/10.1016/j.tca.2015.04.004
0040-6031/

diagram) modeling. Then the glass forming behavior of Co–Hf amorphous alloys will be discussed based on the obtained thermodynamic description of the system.

2. Evaluation of literature information

Both the experimental data published in the literature [5–14,18–23] and those from our previous work [17] are evaluated in this section. All of the data are summarized in Table 1 and concisely categorized as follows.

2.1. Phase diagram information

Using differential thermal analysis (DTA), X-ray diffraction (XRD) and metallographic analysis (MA), Svechnikov et al. [14] and Buschow et al. [12] constructed the Co–Hf phase diagram in the whole composition range and in the Co-rich region, respectively. The liquidus in the Co-rich region measured by both groups agreed well with each other. However, Svechnikov et al. [14] reported four intermetallic phases, viz., $CoHf_2$, CoHf, Co_2Hf, and Co_4Hf, in the phase diagram, while Buschow et al. [12] replaced Co_4Hf with Co_7Hf_2, and proposed another two high-temperature stoichiometric compounds, viz., Co_7Hf and $Co_{23}Hf_6$. The assessed phase diagram by Ishida and Nishizawa [11] was mainly based on the experimental information from Refs. [12,14]. Recently, phase equilibria in the Co-rich region of the Co–Hf phase diagram was re-investigated by the present authors [17] based on the results from XRD, transmission electron microscopy (TEM), scanning electron microscopy (SEM), electron probe microanalysis (EPMA) and differential scanning calorimetry (DSC). The stoichiometry of the reported Co_7Hf was modified to be $Co_{11}Hf_2$ with a stable temperature range from ~650 to 1273 °C. The Co_7Hf_2 phase was excluded from the updated phase diagram, while $Co_{23}Hf_6$ was detected to be stable in a wider temperature range than that reported in the literature. The improvements in the phase relationships agree well with the previous crystallographic studies by Demczyk and Cheng [24] and the first-principles calculations by Levy et al. [23], which questioned the actual composition of Co_7Hf and the stability of Co_7Hf_2 at low temperatures, respectively. Detailed description of the experimental process can be found in our previous work [17].

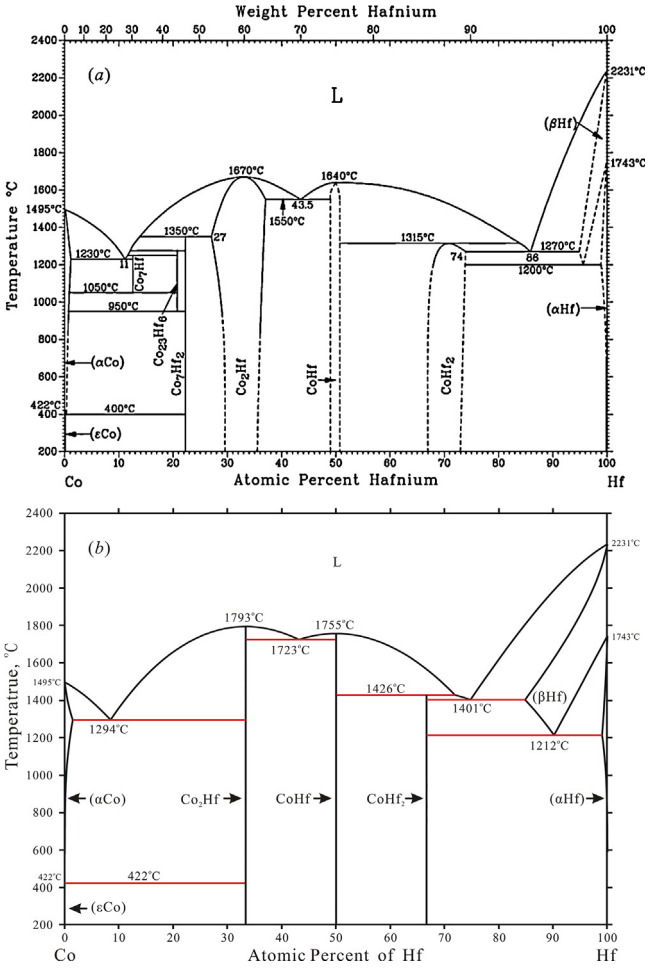

Fig. 1. The Co–Hf phase diagrams (a) assessed by Ishida and Nishizawa and Okamoto [11,15], and (b) calculated using the parameters of Bratberg and Jansson [16].

Properties of the Laves phase Co_2Hf have drawn the attention of several researchers [12–14,22]. The melting point of Co_2Hf was reported to be 1670 and 1620 °C by Svechnikov et al. [14] and Buschow et al. [12], respectively. Considering the higher purity of raw materials used and more detailed description of experimental procedure by Buschow et al. [12], the melting temperature of Co_2Hf is set to be 1620 °C in the present optimization. Aoki et al. [13] determined the homogeneity range of Co_2Hf to be 28.5–33.3 at.% Hf at 1000 °C by lattice parameter measurements, and Chen et al. [22] reported that Co_2Hf was stable from 28 to 35 at.% Hf at 1400 °C based on the results of XRD and EPMA. The composition ranges of Co_2Hf measured by Svechnikov et al. [14] were not included in the current optimization due to the relatively low purity of raw materials used and contradiction with other literature information. Therefore, experimental data by Aoki et al. [13] and Chen et al. [22] as well as those from our previous work [17] were employed in the present modeling, while the data from Ref. [22] received a greater weight for the higher purity of raw materials and more established experimental methods employed.

When the Hf concentration is higher than 33.3 at.% Hf, literature information becomes limited. CoHf was claimed to melt congruently at 1640 °C, and a eutectic reaction, $L \leftrightarrow Co_2Hf + CoHf$, was reported at 1550 °C by Svechnikov et al. [14]. These data were employed in the present optimization with a relatively low weight due to the inaccuracy of the measurements at high temperatures and low purity of the raw materials used. For the Hf concentration in excess of 50 at.% Hf, the phase diagram reported by Svechnikov et al. [14] becomes questionable. The liquidus of primary CoHf extends across a wide composition range of 50–86 at.% Hf, which is too asymmetric compared with that on the other side of the CoHf stoichiometry [25]. By means of SEM, EPMA and DSC, the as-cast microstructures and invariant reaction temperatures were investigated by the present authors [17]. According to the experimental observations, $CoHf_2$ was confirmed to melt through a peritectic reaction $L + CoHf \leftrightarrow CoHf_2$ around 1315 °C, but the eutectic composition for the reaction $L \leftrightarrow CoHf_2 + (\beta Hf)$ was modified to be around 71.5 at.% Hf.

Experimental information for the terminal solution phases ((αCo), (εCo), (αHf) and (βHf)) are relatively limited. The only data available are their terminal solubilities measured in our previous work [17] at 700 and 1100 °C, and the invariant reactions in which they are involved. The thermodynamic parameters for these phases were optimized using these data, as described in Section 5.2.

2.2. Thermodynamic information

Using high temperature calorimeter, Turchanin et al. [6,7] measured the partial and integral enthalpies of mixing of liquid in the composition range of 0–50 at.% Hf at 1650 °C. The integral enthalpies were used to optimize the parameters for liquid in the present modeling, while the partial ones were not included in the

Table 1
Summary of the experimental data for the Co–Hf system.

Type of data	Reference	Experimental method[a]	Quoted mode[b]
Liquidus			
0–33 at.% Hf	[12]	DTA and MA	■
0–100 at.% Hf	[14]	DTA and MA	■
	[17]	DSC and MA	■
Solidus			
In Co-rich region	[14]	DTA and MA	■
In Hf-rich region	[14]	DTA and MA	□
Solubility			
Hf in (αCo)	[17]	EPMA	■
Co in (αHf)	[17]	EPMA	■
Homogeneity of different compounds			
Co_2Hf	[14]	XRD	□
	[13]	XRD	■
	[22]	EPMA and XRD	■
	[17]	EPMA	■
CoHf	[17]	EPMA	■
$CoHf_2$	[17]	EPMA	■
Congruent temperatures	[12]	DTA	■
	[14]	DTA	■
	[8]	DTA	+
Eutectic temperatures	[14]	DTA and MA	■
	[12]	DTA and MA	■
	[17]	DSC and MA	■
Peritectic temperatures	[14]	DTA and MA	■
	[12]	DTA and MA	■
	[17]	DSC and MA	■
Eutectoid temperatures	[14]	DTA	□
	[12]	XRD and MA	+
	[17]	MA	■
Enthalpy of mixing of liquid	[6,7]	High temperature calorimetry	■
Enthalpies of formation	[19]	High temperature calorimetry	□
	[18]	Solute–solvent drop calorimetry	□
	[21]	Direct synthesis calorimetry	■
	[23]	First-principles calculations	■
	This work	First-principles calculations	■
Heat contents of Co_2Hf and $CoHf_2$	This work	Drop calorimetry	■
Heat capacities of $CoHf_2$	[20]	DTA	+

[a] DTA: differential thermal analysis; MA: metallographic analysis; DSC: differential scanning calorimetry; EPMA: electron microprobe microanalysis.
[b] Indicates whether the data are used or not used in the optimization procedure: ■, used; □, not used but considered as reliable data for checking the modeling; +, not used.

assessment procedure, but were used to check the reliability of the optimized parameters.

Enthalpies of formation for the intermetallic phases were measured and calculated by different authors with various methods [18,19,21,23]. By means of high temperature calorimetry, Gachon et al. [19] measured the enthalpies of formation for Co_2Hf, CoHf, $CoHf_2$ at 1300, 1380 and 1100 °C, respectively. Using solute–solvent drop calorimetry technique, Topor and Kleppa [18] obtained the enthalpy of formation for CoHf at 25 °C. Subsequently, Guo and Kleppa [21] re-determined the enthalpies of formation for CoHf as well as Co_2Hf at 25 °C, using direct synthesis calorimetry method. Levy et al. [23] computed the enthalpies of formation for Co_7Hf_2, $CoHf_2$, CoHf and Co_2Hf through first-principles calculations, indicating that Co_7Hf_2 was not stable at low temperature, which agrees with the conclusions drawn in our previous work [17]. Literature information for enthalpies of formation from Refs. [21,23] were included in the present optimization due to their better agreement with each other.

By means of DTA, Ivanovic et al. [20] measured the specific heat of $CoHf_2$ in the temperature range of 2–467 °C. It first increases from 27 to 31 J/mole-atoms-K, and then a pronounced drop starts around 320 °C. This deviation was supposed to be associated with the second order diffuse transition and attributed to the contribution of defect arising preferentially around the 16c position of the $NiTi_2$-type crystal [20]. These values were not employed in the present modeling due to the relatively large inaccuracy of the dynamic DTA technique for thermodynamic property measurements. The heat contents of $CoHf_2$ and Co_2Hf in wider temperature ranges were measured by drop calorimetry techniques with higher accuracy in the present work, as presented in Section 3 and discussed in Section 5.3.

3. Experimental procedure

Co–Hf binary alloys were prepared at the stoichiometries of Co_2Hf and $CoHf_2$ with 99.999 wt.% Co (Jinchuan Group Co., Ltd., China) and 99.99 wt.% Hf (China New Metal Materials Technology

Co., Ltd., China) in an arc melting furnace (WKDHL-I, Opto-electronics Co., Ltd., Beijing, China) under high purity argon atmosphere (1 bar) using a non-consumable W electrode. The ingots were re-melted four times to improve their homogeneities. No chemical analysis for the alloys was conducted since the weight losses of alloys were all less than 0.5 wt.% during arc-melting. Afterwards, the ingots were encapsulated in evacuated silica capsules under vacuum (1 Pa), annealed in an L4514-type diffusion furnace (Qingdao Instrument & Equipment Co., Ltd., China) at 1100 °C for 1080 h and then water-quenched. The annealed alloys were confirmed to be at single-phase state by powder XRD examinations, which were performed using Cu-Kα radiation on a Rigaku D/Max 2250 VB + X-ray diffractometer at 40 kV and 250 mA.

Heat contents of Co_2Hf and $CoHf_2$ were measured by drop calorimetry measurements. The experiments were carried out in an argon atmosphere (1 bar) using a Multi-detector High Temperature Calorimeter Ligne 96 (MHTC 96) from Setaram (Lyon, France) in the temperature range of 300–1200 °C with intervals of 100 °C. At each temperature, five individual measurements were performed for each alloy, and their average was taken to be the experimental value. The standard deviation of the measured values was calculated and defined as their error bars. The accuracy of the temperatures at each point was controlled within ±2 K. Details of the experimental procedure are described elsewhere [26].

4. First-principles calculations for enthalpy of formation

First-principles calculations based on density functional theory (DFT) [27] within generalized gradient approximation (GGA) along with projector augmented-wave (PAW) [28] method were employed to obtain the enthalpy of formation for $Co_{23}Hf_6$, as implemented in the Vienna ab initio simulation package (VASP) [29,30]. The GGA proposed by Perdew et al. [31] was used in the calculation. The atoms were relaxed toward equilibria until the Hartree forces were less than 0.02 eV/Å. A plane-wave cut off energy of 268 eV and an energy convergence criterion of 10^{-6} eV for electronic structure self-consistency were used in the calculations. Brillouin zone integrations were performed using the Monkhorst-Pack [32] k-point meshes scheme, i.e., $3 \times 3 \times 3$ for $Co_{23}Hf_6$, and the total energy differences were converged to within 0.1 kJ/mole-atoms. Both the unit cell sizes and the ionic coordinates were fully relaxed to find the stable state.

The enthalpy of formation ΔH_f is given by the energy of Co_xHf_y relative to the composition-weighted average of the energies of the pure constituents in their equilibrium crystal structures:

$$\Delta H_f = E^{Co_xHf_y} - X_{Co} \times E^{Co} - X_{Hf} \times E^{Hf} \quad (1)$$

where $E^{Co_xHf_y}$, E^{Co} and E^{Hf} are the total energies of Co_xHf_y, Co and Hf, respectively. In the present work, Co_xHf_y represents the $Co_{23}Hf_6$ compound ($cF116$, $Fm\bar{3}m$) at its stoichiometric composition. In addition, the reference states of the pure constituents are hcp Co (ferromagnetic) and hcp Hf (nonmagnetic), respectively, and magnetic contribution to the total energies of $Co_{23}Hf_6$ was considered in the present calculations.

5. Thermodynamic modeling

5.1. Models

5.1.1. Unary phases

The thermodynamic properties of pure elements Co and Hf are taken from the SGTE-compilation by Dinsdale [33] described in the form of:

$$G_i(T) - H_i^{SER} = A + B \times T + C \times T \times \ln T + D \times T^2 + E \times T^{-1} + F \times T^3 + I \times T^7 + J \times T^{-9} \quad (2)$$

where, H_i^{SER} is the molar enthalpy of the element i at 298.15 K and 1 bar in its standard element reference (SER) state, and T is the absolute temperature. The last two terms in Eq. (2) are used only outside the ranges of the melting point, $I \times T^7$ for a liquid below the melting point and $J \times T^{-9}$ for solid phases above the melting point.

5.1.2. Solution phases

The liquid, (αCo), (εCo), and (αHf) phases are modeled as completely disordered solutions, and their molar Gibbs energies are described in the form of:

$$G^{\phi} - H^{SER} = x_{Co} \times {}^0G^{\phi}_{Co} + x_{Hf} \times {}^0G^{\phi}_{Hf} + R \times T \times (x_{Co} \times \ln x_{Co} + x_{Hf} \times \ln x_{Hf}) + x_{Co} \times x_{Hf} \times L^{\phi}_{Co,Hf} + {}^{mag}G^{\phi} \quad (3)$$

where H^{SER} is the abbreviation of $x_{Co} \times H^{SER}_{Co} + x_{Hf} \times H^{SER}_{Hf}$, x_i is the mole fraction of the element i (i = Co or Hf), and ${}^0G^{\phi}_i$ is the Gibbs energy of element i with the state of ϕ. $L^{\phi}_{Co,Hf}$ represents the interaction parameter which has a composition dependence in the form of the Redlich–Kister (R–K) polynomial [34]:

$$L^{\phi}_{Co,Hf} = \sum_{i=0}^{n} L^{i,\phi}_{Co,Hf} \times (x_{Co} - x_{Hf})^i \quad (4)$$

where $L^{i,\phi}_{Co,Hf} = a_i + b_iT$ is the ith interaction parameter of solution phase ϕ in the Co–Hf system, and a_i and b_i are the parameters to be optimized from the experimental phase diagram and thermodynamic data.

It is worth mentioning that the use of the R–K polynomial assumes a linear T-dependence of the interaction energy of the liquid phase, which means a constant heat of mixing and excess entropy of mixing, as well as zero excess heat capacity for the liquid phase in the whole temperature range. According to the work of Kaptay [35,36], the contribution of excess heat capacity to the interaction energy of the liquid phase can barely be ignored. In this point of view, the description of the liquid phase in the present work is a simplified treatment. However, since the thermodynamic information for the liquid phase is limited, and the main interest of the present work lies on the phase relationships among the solid phases at relatively low temperatures, we choose to employ the simplified R–K polynomial to describe the interaction energy of the liquid phase. The rationality of our preference can be confirmed by the calculations, as present in Section 5.3.

The last term in Eq. (3) is the magnetic contribution to the Gibbs energy. For the liquid phase, ${}^{mag}G^{\phi}$ is equal to zero, and for other solution phases, the magnetic contribution from pure Co to the Gibbs energy is given by the Hillert–Jarl–Inden model [37,38]:

$$G^{mag}_m = R \times T \times \ln\left(\beta^{\phi} + 1\right) \times g\left(\tau^{\phi}\right) \quad (5)$$

in which β is the Bohr magnetic moment per mole of atoms, and $\tau = T/T^*$, T^* is defined as the critical temperature for magnetic ordering (Curie or Neel temperature). The complete description of the function $g(\tau)$ is given in Ref. [37], and the parameters T_c and β for pure element Co can be found in Ref. [33]. Due to the lack of experimental data, the magnetic interaction parameter between Co and Hf was not used in the present modeling.

5.1.3. Intermetallic compounds

According to the experimental observations in our previous work [17], five intermetallic phases, viz., $Co_{11}Hf_2$, $Co_{23}Hf_6$, Co_2Hf, CoHf and $CoHf_2$, exist in the Co–Hf system. The Gibbs energy per mole atoms of $Co_xHf_{(1-x)}$ compound is described by:

$$ {}^{0}G_{m}^{Co_xHf_{(1-x)}} - x \times H_{Co}^{SER} - (1-x) \times H_{Hf}^{SER} = A + B \times T $$
$$ + x \times {}^{0}G_{Co}^{hcp} + (1-x) \times {}^{0}G_{Hf}^{hcp} \quad (6) $$

in which, A and B are the parameters to be evaluated in the course of optimization.

In the view of the reported homogeneity ranges [13,14,22], the Laves phase Co_2Hf and $NiTi_2$-typed phase $CoHf_2$ are described with two-sublattice models, $(Co, Hf)_x(Co, Hf)_y$, with the first sublattice mainly occupied by Co and the second by Hf, and x, y denote the number of sites in each sublattice with $x+y=1$. Their molar Gibbs energy functions are expressed as:

$$ \begin{aligned} {}^{0}G^{\phi} &= y'_{Co} \times y''_{Hf} \times {}^{0}G^{\phi}_{Co:Hf} + y'_{Co} \times y''_{Co} \times {}^{0}G^{\phi}_{Co:Co} + y'_{Hf} \times y''_{Hf} \\ &\times {}^{0}G^{\phi}_{Hf:Hf} + y'_{Hf} \times y''_{Co} \times {}^{0}G^{\phi}_{Hf:Co} + x \times R \times T \\ &\times (y'_{Co} \times \ln y'_{Co} + y'_{Hf} \times \ln y'_{Hf}) + y \times R \times T \\ &\times (y''_{Co} \times \ln y''_{Co} + y''_{Hf} \times \ln y''_{Hf}) + y'_{Co} \times y''_{Co} \times y''_{Hf} \\ &\times {}^{0}L^{\phi}_{Co:Co,Hf} + y'_{Hf} \times y''_{Co} \times y''_{Hf} \times {}^{0}L^{\phi}_{Hf:Co,Hf} + y'_{Co} \times y'_{Hf} \\ &\times y''_{Co} \times {}^{0}L^{\phi}_{Co,Hf:Co} + y'_{Co} \times y'_{Hf} \times y''_{Hf} \times {}^{0}L^{\phi}_{Co,Hf:Hf} + \cdots \end{aligned} \quad (7) $$

where the parameters y'_i and y''_i are the site fractions of the component of i (i = Co or Hf) on the first and second sublattice, respectively. ${}^{0}G^{\phi}_{Co:Hf}$ is the Gibbs energy of the ideal compound Co_xHf_y, which is described by Eq. (6). According to the Wagner–Schottky model [39], ${}^{0}G^{\phi}_{Co:Co}$ and ${}^{0}G^{\phi}_{Hf:Hf}$ correspond to the Gibbs energy needed to fill one sublattice with anti-structure defects. A value of 5000 J/mole-atoms is assigned to ${}^{0}G^{\phi}_{Co:Co}$ and ${}^{0}G^{\phi}_{Hf:Hf}$ relative to the Gibbs energy of Co and Hf at their reference states, i.e., ${}^{0}G^{\phi}_{Co:Co} - {}^{0}G^{hcp}_{Co} = 5000$ and ${}^{0}G^{\phi}_{Hf:Hf} - {}^{0}G^{hcp}_{Hf} = 5000$ (ϕ = Co_2Hf or $CoHf_2$). The parameter ${}^{0}G^{\phi}_{Hf:Co}$ relates to filling both sublattices with anti-structure defects, and can be estimated by the equation ${}^{0}G^{\phi}_{Hf:Co} = {}^{0}G^{\phi}_{Co:Co} + {}^{0}G^{\phi}_{Hf:Hf} - {}^{0}G^{\phi}_{Co:Hf}$. In addition, the following equations are adapted by assuming that the interaction between two species in one sublattice is independent of the occupation on the other:

$$ {}^{0}L^{\phi}_{Co:Co,Hf} = {}^{0}L^{\phi}_{Hf:Co,Hf} = {}^{0}L^{\phi}_{*:Co,Hf}\ {}^{0}L^{\phi}_{Co,Hf:Co} = {}^{0}L^{\phi}_{Co,Hf:Hf} = {}^{0}L^{\phi}_{Co,Hf:*} \quad (8) $$

5.1.4. B2 and A2 phases

The equiatomic compound CoHf is reported to have an ordered B2 structure [40], and an MSL model with two symmetric sublattices, $(Co,Hf,Va)_{0.5}(Co,Hf,Va)_{0.5}$, was employed to describe the B2 phase. Correspondingly, the high temperature A2 phase (βHf) was described with a one-sublattice model $(Co,Hf,Va)_1$. The molar Gibbs energy of the ordered B2 phase and disordered A2 phase can be expressed by using a single equation:

$$ G^{B2} = {}^{dis}G^{A2}(x_i) + {}^{ord}G^{B2}(y_i^1, y_i^2) - {}^{ord}G^{B2}(x_i) \quad (9) $$

where the mole fraction x_i and the site fraction y_i^1 and y_i^2 are related according to $x_i = 0.5y_i^1 + 0.5y_i^2$ (i = Co or Hf).

In Eq. (9), the first term ${}^{dis}G^{A2}(x_i)$ is the molar Gibbs energy of the disordered A2 phase, which is regarded as a substitutional solution with the same mathematical expression as Eq. (3). However, the introduction of the vacancies into the sublattice brings about additional parameters. First, ${}^{0}G^{A2}_{Va}$ represents the energy to form thermal vacancies, which are not considered in the present treatment. Thus, ${}^{0}G^{A2}_{Va}$ is set to be a highly positive value of $30T$ to keep the vacancy fraction low at all temperatures [41]. Second, the interaction parameters $L^{A2}_{Co,Va}$ and $L^{A2}_{Hf,Va}$ are fixed to be 146588.8 and 150446.4, respectively. These values were derived from the enthalpy of formation for monovacancies in pure Co and Hf by assuming the equality of $L^{A2}_{i,Va}$ to $\Delta^{f}H^{i}_{Va}$ values at bcc state. The

Table 2
Summary of the thermodynamic parameters in the Co–Hf system.[a]

Liquid: model $(Co,Hf)_1$
- ${}^{0}L^{L}_{Co,Hf} = -166619.477 + 33.2126304 \times T$
- ${}^{1}L^{L}_{Co,Hf} = +4263.91640 - 9.1089 \times T$
- ${}^{2}L^{L}_{Co,Hf} = +4130.46576$

(αCo) (A1): model $(Co,Hf)_1(Va)_1$
- ${}^{0}L^{A1}_{Co,Hf:Va} = -61205.4988$

(βHf) (A2): model $(Co,Hf,Va)_1(Va)_3$
- ${}^{0}G^{A2}_{Va:Va} = +30 \times T$[b]
- ${}^{0}L^{A2}_{Co,Hf:Va} = -100060.0 + 21.50645 \times T$
- ${}^{0}L^{A2}_{Co,Va:Va} = +146588.8$[b]
- ${}^{0}L^{A2}_{Hf:Va:Va} = +150446.4$[b]

CoHf (B2): model $(Co,Hf,Va)_{0.5}(Co,Hf,Va)_{0.5}(Va)_3$
- ${}^{0}G^{B2}_{Co:Co:Va} = {}^{0}G^{B2}_{Hf:Hf:Va} = {}^{0}G^{B2}_{Va:Va:Va} = 0$
- ${}^{0}G^{B2}_{Co:Hf:Va} = {}^{0}G^{B2}_{Hf:Co:Va} = -50898.5527 + 5.4982 \times T$
- ${}^{0}G^{B2}_{Co:Va:Va} = {}^{0}G^{B2}_{Va:Co:Va} = +73294.4$[b]
- ${}^{0}G^{B2}_{Hf:Va:Va} = {}^{0}G^{B2}_{Va:Hf:Va} = +75223.2$[b]
- ${}^{0}L^{B2}_{Co,Hf:Co:Va} = {}^{0}L^{B2}_{Co:Co,Hf:Va} = -26980.5$
- ${}^{0}L^{B2}_{Co,Hf:Hf:Va} = {}^{0}L^{B2}_{Hf:Co,Hf:Va} = +29005.8$

(εCo) and (αHf) (A3): model $(Co,Hf)_1(Va)_{0.5}$
- ${}^{0}L^{A3}_{Co,Hf:Va} = -39372.6592 + 4.24066589 \times T$

$Co_{11}Hf_2$: model $(Co)_{0.8462}(Hf)_{0.1538}$
- ${}^{0}G^{Co_{11}Hf_2}_{Co:Hf} - 0.8462\,{}^{0}G^{hcp}_{Co} - 0.1538\,{}^{0}G^{hcp}_{Hf} = -25931.56 + 4.63242531 \times T$

$Co_{23}Hf_6$: model $(Co)_{0.7931}(Hf)_{0.2069}$
- ${}^{0}G^{Co_{23}Hf_6}_{Co:Hf} - 0.7931\,{}^{0}G^{hcp}_{Co} - 0.2069\,{}^{0}G^{hcp}_{Hf} = -33844.173 + 6.02 \times T$

Co_2Hf: model $(Co,Hf)_{0.6667}(Co,Hf)_{0.3333}$
- ${}^{0}G^{Co_2Hf}_{Co:Hf} - 0.6667\,{}^{0}H^{SER}_{Co} - 0.3333\,{}^{0}H^{SER}_{Hf} = -45149.435 + 6.3705 \times T + 0.6667\,{}^{0}G^{hcp}_{Co} + 0.3333\,{}^{0}G^{hcp}_{Hf}$

- ${}^{0}G^{Co_2Hf}_{Co:Co} = {}^{0}G^{hcp}_{Co} + 5000$[b]
- ${}^{0}G^{Co_2Hf}_{Hf:Hf} = {}^{0}G^{hcp}_{Hf} + 5000$[b]
- ${}^{0}G^{Co_2Hf}_{Hf:Co} = {}^{0}G^{Co_2Hf}_{Co:Co} + {}^{0}G^{Co_2Hf}_{Hf:Hf} - {}^{0}G^{Co_2Hf}_{Co:Hf}$
- ${}^{0}L^{Co_2Hf}_{*:Co,Hf} = -26267.3173 + 13.2339241 \times T$
- ${}^{0}L^{Co_2Hf}_{Co,Hf:*} = -5887.60442$

$CoHf_2$: model $(Co,Hf)_{0.3333}(Co,Hf)_{0.6667}$
- ${}^{0}G^{CoHf_2}_{Co:Hf} - 0.3333\,{}^{0}H^{SER}_{Co} - 0.6667\,{}^{0}H^{SER}_{Hf} = -33120.5404 + 4.7703 \times T + 0.3333\,{}^{0}G^{hcp}_{Co} + 0.6667\,{}^{0}G^{hcp}_{Hf}$

- ${}^{0}G^{CoHf_2}_{Co:Co} = {}^{0}GCo^{hcp} + 5000$[b]
- ${}^{0}G^{CoHf_2}_{Hf:Hf} = {}^{0}GHf^{hcp} + 5000$[b]
- ${}^{0}G^{CoHf_2}_{Hf:Co} = {}^{0}G^{CoHf_2}_{Co:Co} + {}^{0}G^{CoHf_2}_{Hf:Hf} - {}^{0}G^{CoHf_2}_{Co:Hf}$
- ${}^{0}L^{CoHf_2}_{*:Co,Hf} = -42302.5$
- ${}^{0}L^{CoHf_2}_{Co,Hf:*} = +7501.7$

[a] Temperature (T) in Kelvin and Gibbs energy in J/mole.
[b] Fixed parameters during the optimization.

values of $\Delta^f H^{Co}_{Va} = 146.588$ kJ/mole-atoms and $\Delta^f H^{Hf}_{Va} = 150.4464$ kJ/mole-atoms at bcc state were computed by Korzhavyi et al. [42] through first-principles calculations, which were compatible with other parameters during the optimization procedure. The following two terms in Eq. (9) are the ordering contributions, which are calculated using the Eq. (10) below:

$$\begin{aligned} {}^{ord}G^{B2}(y^1_i, y^2_i) &= y^1_{Co} \times y^2_{Hf} \times G^{B2}_{Co:Hf} + y^1_{Hf} \times y^2_{Co} \times G^{B2}_{Hf:Co} + y^1_{Co} \\ &\times y^2_{Va} \times G^{B2}_{Co:Va} + y^1_{Va} \times y^2_{Co} \times G^{B2}_{Va:Co} + y^1_{Hf} \times y^2_{Va} \times G^{B2}_{Hf:Va} \\ &+ y^1_{Va} \times y^2_{Hf} \times G^{B2}_{Va:Hf} + 0.5R \times T \\ &\times (y^1_{Co} \times \ln y^1_{Co} + y^1_{Hf} \times \ln y^1_{Hf} + y^1_{Va} \times \ln y^1_{Va} + y^2_{Co} \times \ln y^2_{Co} \\ &+ y^2_{Hf} \times \ln y^2_{Hf} + y^2_{Va} \times \ln y^2_{Va}) + y^1_{Co} \times y^1_{Hf} \times y^2_{Co} \times L^{B2}_{Co,Hf:Co} \\ &+ y^1_{Co} \times y^2_{Co} \times y^2_{Hf} \times L^{B2}_{Co:Co,Hf} + y^1_{Co} \times y^1_{Hf} \times y^2_{Hf} \times L^{B2}_{Co,Hf:Hf} \\ &+ y^1_{Hf} \times y^2_{Co} \times y^2_{Hf} \times L^{B2}_{Hf:Co,Hf} \end{aligned} \quad (10)$$

${}^{ord}G^{B2}(y^1_i, y^2_i)$ was first calculated with the site fraction y^1_i and y^2_i, and then using the same model parameters but replacing y^1_i and y^2_i with mole fraction x_i, ${}^{ord}G^{B2}(x_i)$\ can be obtained. When the phase becomes completely disordered, i.e., $y^1_i = y^2_i = x_i$, the second and third terms in Eq. (9) will cancel each other, and only the first term ${}^{dis}G^{A2}(x_i)$\ will give a contribution to the Gibbs energy.

For the B2 MSL description, $G^{B2}_{Co:Va}$ and $G^{B2}_{Hf:Va}$ are fixed at 73294.4 and 75223.2, respectively, by assuming the equality to half of the enthalpy of formation for monovacancies in pure components [42]. The parameters $G^{B2}_{Co:Hf}$, $L^{B2}_{Co,Hf:Co}$ and $L^{B2}_{Co,Hf:Hf}$ are to be optimized according to the experimental data.

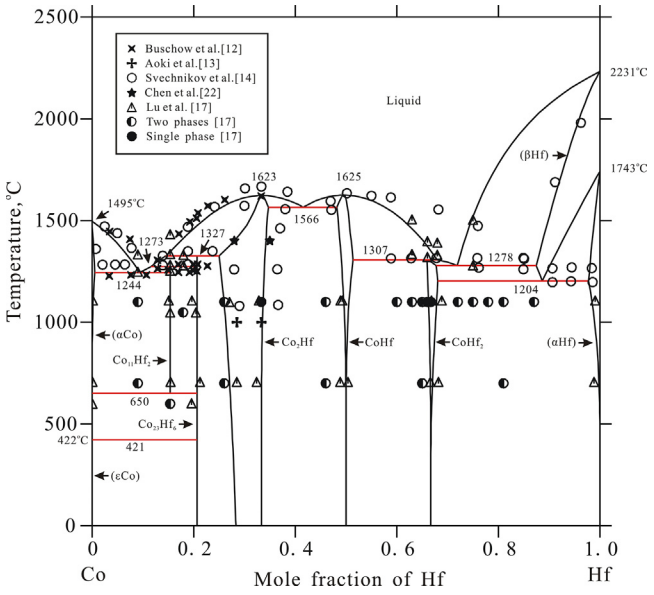

Fig. 2. The calculated Co–Hf phase diagram along with the experimental data from our previous work [17] and the literature [12–14,22].

5.2. Optimization procedure

The optimization of the thermodynamic parameters for the Co–Hf system was performed using the PARROT module of the Thermo-Calc software [43], following a step-by-step optimization strategy described by Du et al. [44]. The optimization started with the liquid phase, using the zeroth order interaction parameters to

Table 3
Summary of the invariant equilibria in the Co–Hf system.

Reaction	Type	Composition (at.% Hf)			T (°C)	Reference	Method[a]
Liquid ↔ CoHf	Congruent	50	50		1640 ± 20	[14]	DTA
		49.56	49.56		1625	This work	Calculated
Liquid ↔ Co_2Hf	Congruent	33.33	33.33		1670 ± 20	[14]	DTA
		33.33	33.33		1620	[12]	DTA
		33.45	33.45		1623	This work	Calculated
Liquid ↔ Co_2Hf + CoHf	Eutectic	43.5	37.5	~49	1550 ± 20	[14]	DTA
		41.91	34.28	47.16		[17]	MA
		41.53	34.68	48.21	1566	This work	Calculated
Liquid + Co_2Hf ↔ $Co_{23}Hf_6$	Peritectic	13.5	27	–	~1350	[12]	MA
					1350 ± 20	[14]	DTA
					1326	[17]	DSC
		14.54	25.01	20.69	1327	This work	Calculated
Liquid + CoHf ↔ $CoHf_2$	Peritectic	84	~50.5	~71	1315 ± 20	[14]	DTA
		~69			1312.8	[17]	MA, DSC
		67.95	51.41	65.94	1307	This work	Calculated
Liquid ↔ $CoHf_2$ + (βHf)	Eutectic	86	74	~95	1270 ± 20	[14]	DTA
		~71.5			1271.1	[17]	MA, DSC
		71.91	67.72	87.47	1278	This work	Calculated
Liquid + $Co_{23}Hf_6$ ↔ $Co_{11}Hf_2$	Peritectic				1275	[12]	DTA
					1273	[17]	DSC
		11.61	20.69	15.38	1273	This work	Calculated
Liquid ↔ (αCo) + $Co_{11}Hf_2$	Eutectic	11	~1.5		1280 ± 20	[14]	DTA
					1230	[12]	DTA
		9.65		15.38	1245.3	[17]	MA, DSC
		9.44	~0	15.38	1244	This work	Calculated
(βHf) ↔ $CoHf_2$ + (αHf)	Eutectoid	~96	~74	~99	1200 ± 20	[14]	DTA
		88.62	68.04	97.78	1204	This work	Calculated
$Co_{11}Hf_2$ ↔ (αCo) + $Co_{23}Hf_6$	Eutectoid				650 ± 50	[17]	MA
		15.38	~0	20.69	650	This work	Calculated
(αCo) ↔ (εCo) + $Co_{23}Hf_6$	Eutectoid	~0.5	~0.4		400	[14]	Assessed
		~0	~0	20.69	421	This work	Calculated

[a] DTA: differential thermal analysis; MA: metallographic analysis; DSC: differential scanning calorimetry.

fit the measured integral enthalpies of mixing. Subsequently, intermetallic compounds and the other solution phases were introduced into the modeling one by one. At the beginning, all the intermetallic phases were treated as stoichiometric compounds, and the enthalpies of formation for the intermetallic phases were used as good starting values for A in Eq. (6). Parameters A and B were adjusted to describe the enthalpies of formation, liquidus and invariant reactions. Afterwards, parameters for the solution phases were introduced to describe the solubility ranges according to the measured terminal solubilities and the invariant reactions in which they are involved. During this procedure, the first and second order interaction parameters of the liquid phase, viz., a_1, b_1 and a_2 in Eq. (3), were introduced to describe the complex shape of liquidus in the phase diagram. When the calculated invariant temperatures were adjusted within the claimed error ranges, sublattice models were introduced to describe the composition ranges of Co_2Hf and $CoHf_2$. Finally, the order–disorder transition between B2 (CoHf) and A2 (βHf) was taken into account, and all parameters for different phases were optimized simultaneously to achieve a globally self-consistent thermodynamic description. The finally obtained thermodynamic parameters are listed in Table 2.

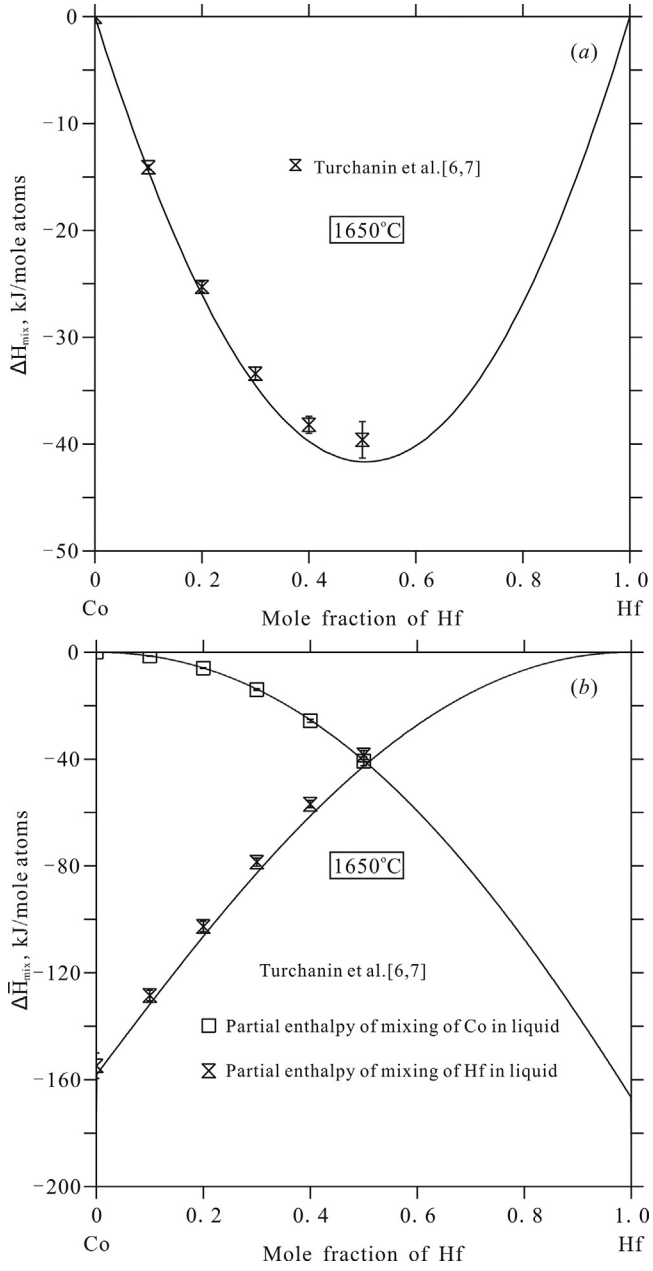

Fig. 3. The calculated (a) integral and (b) partial molar enthalpies of mixing for liquid at 1650 °C along with the experimental values from the literature [6,7].

5.3. Optimization results

The calculated Co–Hf phase diagram using the presently optimized parameters is presented in Fig. 2, and compared with the experimental data from Refs. [12–14,22] as well as those from our previous work [17]. Table 3 displays the calculated invariant temperatures along with the experimental ones. As shown in the figure, a satisfactory agreement between the calculated phase diagram and the experimental data has been achieved. Especially, no liquid miscibility gap was observed within the defined temperature range of the SGTE database (298.15–6000 K) [33] in the present calculations, which confirms the rationality of using R–K polynomial to describe the excess Gibbs energy of the liquid phase. The Hf-rich liquidus and the eutectic point of ~71.5 at.% Hf for the invariant reaction $L \leftrightarrow CoHf_2 + (\beta Hf)$, which were determined in our previous work [17], can be well reproduced. Visible deviation can be detected on the Co-rich liquidus, which is caused by the symmetry of liquidus and different weights given to the experimental data during optimization. The present optimization result is the tradeoff between phase diagram and thermodynamic data.

Fig. 3 presents the comparison between calculated integral and partial molar enthalpies of mixing for liquid at 1650 °C and those from literature [6,7]. The fit to the experimental data is fairly good, even though the measured partial enthalpies were not included during the optimization procedure.

Fig. 4 shows the calculated enthalpies of formation for different intermetallic phases at 25 °C, together with the reported values by experimental measurements as well as first-principles calculations [18,19,21,23]. The presently calculated enthalpy of formation for $Co_{23}Hf_6$ is −24 kJ/mole-atoms. The result is consistent with the trend of published data for other intermetallic compounds, which supports the conclusions drawn in our previous work [17] that

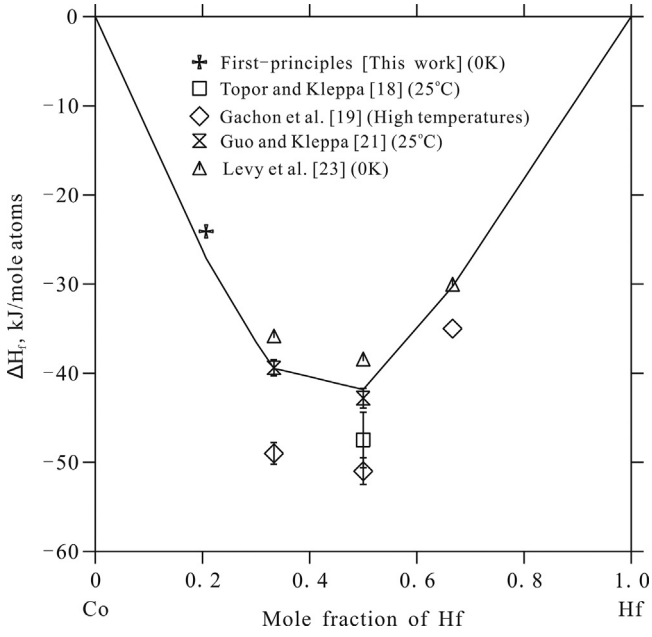

Fig. 4. The calculated enthalpies of formation for different intermetallic phases at 25 °C, together with the reported values from the present work and the literature [18,19,21,23].

$Co_{23}Hf_6$ is stable in a wider temperature range than that reported in the literature.

Fig. 5(a and b) gives the comparison between the measured heat contents and the calculated values for $CoHf_2$ and Co_2Hf, respectively. The measured heat contents together with the corresponding error bars are also presented in Table 4. The thermodynamic models for the intermetallic phases employed in the present assessment are derived from the Neumann–Kopp rule [41]. The good agreement between the calculated and measured values indicates that the models employed in the present assessment are efficient enough to describe the thermodynamic properties of $CoHf_2$ and Co_2Hf.

6. Glass forming behavior

The glass forming behavior of Co–Hf alloys has been investigated by several authors [5–10]. By means of melt spinning technique and DSC, Buschow and Beekmans [10] prepared three Co–Hf amorphous alloys, $Co_{91}Hf_9$, $Co_{40}Hf_{60}$ and $Co_{22}Hf_{78}$ (at.%) and measured the crystallization temperatures (T_x) to be 555, 550 and 485 °C, respectively. Using the same methods, Jansson and Nygren [8] reported the T_x of a $Co_{33}Hf_{67}$ (at.%) alloy to be 503 °C with a crystallization heat of 9.0 kJ/mole-atoms. Afterwards, Politis [9] synthesized Co–Hf amorphous alloys using the mechanical alloying method, and determined the glass forming range (GFR) of the Co–Hf alloys to be 10–85 at.% Hf with a T_x range of 467–560 °C by combining XRD and DSC measurements. Previous experimental investigations on glass transition temperature (T_g) in

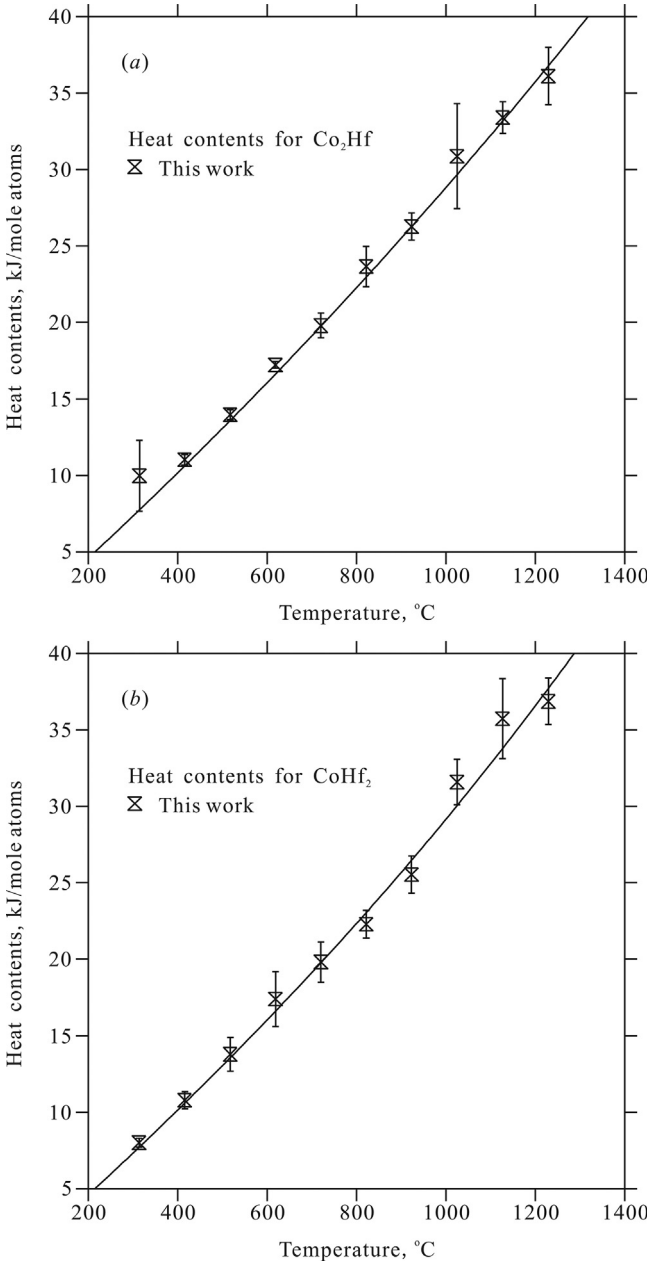

Fig. 5. The calculated heat contents for (a) $CoHf_2$ and (b) Co_2Hf along with the measured values in the present work.

Table 4
Measured heat contents of Co_2Hf and $CoHf_2$ in the present work.[a]

Phase	Temperature[b] (°C)	Heat contents (kJ/mole atoms)	Error bar[c] (kJ/mole atoms)
Co_2Hf	314.60	9.9867	±2.32
	415.76	11.0297	±0.34
	517.55	13.9756	±0.33
	618.68	17.2277	±0.22
	720.28	19.7983	±0.81
	821.56	23.6661	±1.32
	923.22	26.2749	±0.89
	1024.81	30.8695	±3.44
	1127.12	33.4084	±1.04
	1229.17	36.1185	±1.88
$CoHf_2$	313.70	8.0099	±0.29
	415.93	10.7868	±0.56
	517.67	13.7901	±1.10
	618.94	17.3985	±1.81
	720.39	19.8192	±1.32
	821.79	22.2907	±0.91
	923.04	25.5361	±1.21
	1024.86	31.5859	±1.48
	1126.67	35.7274	±2.61
	1229.13	36.8657	±1.52

[a] The experiments were performed in an argon atmosphere under the pressure of 1 bar with the reference temperature of 298.15 K.
[b] The accuracy of the temperatures at each point was controlled within ±2 K.
[c] The error bars were defined as the standard deviations of the five experimental values measured at each temperature.

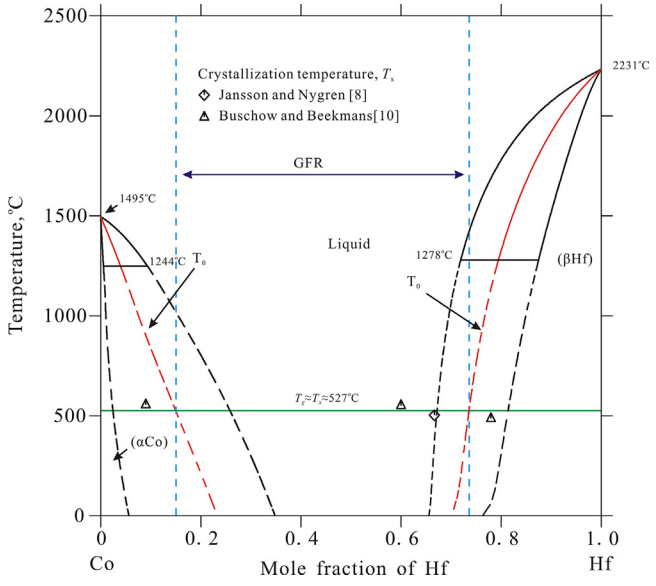

Fig. 6. The calculated metastable phase diagram containing the liquidus, solidus and T_0 curves for the Co–Hf system using the optimized parameters in the present work, together with the measured T_x from the literature [8,10].

the early-transition-metal/late-transition-metal amorphous alloys [45] have shown that T_g is within 50 °C of T_x, so it is customary to approximate T_g with T_x in the absence of T_g information [46]. Therefore, the glass transition temperature of Co–Hf amorphous alloys was approximated to be 527 °C (800 K) according to the measurements by Politis [9].

According to the T_0 criterion proposed by Schwarz et. al [46], the GFR of amorphous alloys that are prepared through rapid quenching can be described by the glass transition temperature T_g and T_0 curves, which are the temperature–composition locus of the equality between the free energies of the liquid and crystal phases. In the regions where $T_0 < T_g$, when the liquid temperature is above T_0, the partitionless crystallization is impossible thermodynamically, and the glass formation would be favored.

Fig. 6 presents the metastable phase diagram of the Co–Hf system with the liquidus, solidus and T_0 curves calculated from the parameters of liquid, (αCo) and (βHf) phases obtained in the present work. The solid curves correspond to the equilibrium regimes above the invariant temperatures, while the dashed ones are extrapolations into metastable regions. By approximating T_g to be 527 °C, the predicted GFR of the Co–Hf amorphous alloys was 15–75 at.% Hf, as shown in Fig. 6.

It is worth mentioning that the predicted GFR is slightly narrower than that measured by Politis [9], who reported a GFR of 10–85 at.% Hf using mechanically alloyed amorphous Co–Hf powders. Three possible reasons can be attributed for the deviation between the predicted values and the experimental observations. Firstly, T_0 criterion does not consider kinetic constraints because it assumes that the partitionless crystallization occurs instantaneously once it is thermodynamically favored [47], however, these constraints cannot be ignored in practical solidification process. Secondly, the amorphous powders prepared by Politis [9] were synthesized through mechanical alloying. Compared with rapid solidification, the method of mechanical alloying is more efficient in producing amorphous alloys. Thirdly, although the R–K polynomial employed for the liquid phase can reproduce satisfactory data in the equilibrated phase diagram, it is essentially a simplified model, and may result in some deviation when extrapolated into the lower temperatures [35,36]. All these reasons ultimately result in the underestimation of the GFR of the Co–Hf amorphous alloys in the present work. Nevertheless, the predicted GFR still fits the experimental observations reasonably, and can provide instructive information for novel bulk amorphous materials design.

7. Summary

All the experimental phase diagram and thermodynamic data available for the Co–Hf system have been critically evaluated. Heat content values of Co_2Hf and $CoHf_2$ were obtained through drop calorimetry measurements. The enthalpy of formation for $Co_{23}Hf_6$ at 0 K was calculated via first-principles calculations.

A set of self-consistent thermodynamic parameters for the Co–Hf system was obtained by considering the present results and critically assessed literature data. The comprehensive comparison shows that the calculated phase diagram and thermodynamic properties are in a good agreement with the experimental data and first-principles calculations.

On the basis of the present thermodynamic description, the GFR of the Co–Hf alloys was predicted based on the T_0 criterion and possible reasons for the deviation from the experimental measurements were analyzed.

Acknowledgements

The financial support from the National Science Foundation for Youth of China (Grant No. 51101172), the National Basic Research Program of China (Grant No. 2011CB610401) and the Sino-German Cooperation Group "Microstructure in Al alloys" (Grant No. GZ755) are greatly acknowledged. One of the authors Xingxu Lu is also grateful to Prof. M. Turchanin for sharing their experimental data on the enthalpies of mixing of the liquid phase.

Appendix A. Supplementary data

Supplementary data associated with this article can be found, in the online version, at http://dx.doi.org/10.1016/j.tca.2015.04.004.

References

[1] W.O. Soboyejo, T.S. Srivatsan, Advanced Structural Materials: Properties, Design Optimization, and Applications, Taylor & Francis, 2006.
[2] S. Kobayashi, Y. Tsukamoto, T. Takasugi, The effects of alloying elements (Ta, Hf) on the thermodynamic stability of γ′-Co_3(Al,W) phase, Intermetallics 31 (2012) 94–98.
[3] S. Kobayashi, Y. Tsukamoto, T. Takasugi, H. Chinen, T. Omori, K. Ishida, S. Zaefferer, Determination of phase equilibria in the Co-rich Co–Al–W ternary system with a diffusion-couple technique, Intermetallics 17 (2009) 1085–1089.
[4] J. Sato, T. Omori, K. Oikawa, I. Ohnuma, R. Kainuma, K. Ishida, Cobalt-base high-temperature alloys, Science 312 (2006) 90–91.
[5] H. Li, X. Lu, Y. Liu, R. Wu, H. Yin, M. Han, G. Chen, Thermodynamic calculation of glass formation for Co–ETM alloys based on Miedema's model, Phys. B (Amsterdam, Netherlands) 413 (2013) 24–30.
[6] M.A. Turchanin, P.G. Agraval, Enthalpies of mixing of titanium, zirconium and hafnium liquid alloys with cobalt, Rasplavy 2 (2002) 8–16.
[7] I.V. Turchanin, P.G. Belokonenko, Enthalpies of formation of liquid binary Co + (Ti, Zr, and Hf) alloys, Conference Progress in Computing of Physicochemical Properties, Warshaw, Poland, 1999.
[8] K. Jansson, M. Nygren, Investigation of the thermal stability and crystallization process of amorphous hafnium–cobalt–nickel ($Hf_{0.67}Co_{0.33-x}Ni_x$) alloys with $0 \le x \le 0.33$ by differential scanning calorimetry and X-ray diffraction, J. Less-Common Met. 171 (1991) 369–375.
[9] C. Politis, Synthesis and characterization of amorphous and microcrystalline materials by mechanical alloying, Z. Phys. Chem. (Munich) 157 (1988) 209–213.
[10] K.H.J. Buschow, N.M. Beekmans, Formation, decomposition, and electrical transport properties of amorphous hafnium–nickel and hafnium–cobalt alloys, J. Appl. Phys. 50 (1979) 6348–6352.
[11] K. Ishida, T. Nishizawa, The Co–Hf (cobalt–hafnium) system, J. Phase Equilib. 12 (1991) 424–427.
[12] K.H.J. Buschow, J.H. Wernick, G.Y. Chin, Note on the hafnium–cobalt phase diagram, J. Less-Common Met. 59 (1978) 61–67.
[13] Y. Aoki, T. Nakamichi, H. Yamamoto, Magnetic susceptibility of the Laves-phase hafnium–cobalt ($HfCo_2$) in the single-phase region, Phys. Status Sol. B 56 (1973) K17–K20.
[14] V.N. Svechnikov, A.K. Shurin, G.P. Dmitrieva, Hafnium–cobalt phase diagram, Izv. Akad. Nauk SSSR Met. 1 (1969) 214–218.
[15] H. Okamoto, Desk Handbook: Phase Diagrams for Binary Alloys, ASM, International, Material Park, Ohio, USA, 2000.
[16] J. Bratberg, B. Jansson, Thermodynamic evaluation of the C–Co–W–Hf–Zr system for cemented carbides applications, J. Phase Equilib. Diff. 27 (2006) 213–219.
[17] X. Lu, K. Cheng, S. Liu, K. Li, F. Zheng, Y. Du, Experimental investigation of phase equilibria in the Co–Hf system, J. Alloys Compd. 627 (2015) 251–260.
[18] L. Topor, O.J. Kleppa, Enthalpies of formation of equiatomic compounds of titanium, zirconium and hafnium with late transition metals: systematic aspects and comparisons with predicted values, J. Less-Common Met. 155 (1989) 61–73.
[19] J.C. Gachon, N. Selhaoui, B. Aba, J. Hertz, Comparison between measured and predicted enthalpies of formation, J. Phase Equilib. 13 (1992) 504–506.
[20] N. Ivanovic, D. Rodic, B. Cekic, M. Manasijevic, S. Koicki, D. Babic, R. Nikolic, Specific heat of the Hf_2Fe, Hf_2Co, and Hf_2Rh intermetallic compounds, J. Mater. Sci. 30 (1995) 3547–3551.
[21] Q. Guo, O.J. Kleppa, Standard enthalpies of formation of some alloys formed between group IV elements and group VIII elements, determined by high-temperature direct synthesis calorimetry II. Alloys of (Ti, Zr, Hf) with (Co, Ni), J. Alloys Compd. 269 (1998) 181–186.
[22] K.C. Chen, E.J. Peterson, D.J. Thoma, $HfCo_2$ Laves phase intermetallics-part I: solubility limits and defect mechanisms, Intermetallics 9 (2001) 771–783.
[23] O. Levy, G.L.W. Hart, S. Curtarolo, Hafnium binary alloys from experiments and first principles, Acta Mater. 58 (2010) 2887–2897.
[24] B.G. Demczyk, S.F. Cheng, Structures of zirconium–cobalt (Zr_2Co_{11}) and hafnium–cobalt ($HfCo_7$) intermetallic compounds, J. Appl. Crystallogr. 24 (1991) 1023–1026.
[25] H. Okamoto, T.B. Massalski, Correct and incorrect phase diagram features, in: J. C. Zhao (Ed.), Methods for Phase Diagram Determination, Elsevier Science Ltd., Oxford, 2007, pp. 51–107 (Chapter 3).

[26] R. Hu, P. Nash, Q. Chen, L. Zhang, Y. Du, Heat capacities of several Al–Ni–Ti compounds, Thermochim. Acta 486 (2009) 57–65.
[27] W. Kohn, L.J. Sham, Self-consistent equations including exchange and correlation effects, Phys. Rev. 140 (1965) A1133–A1138.
[28] P.E. Bloechl, Projector augmented-wave method, Phys. Rev. B: Condens. Matter 50 (1994) 17953–17979.
[29] G. Kresse, J. Furthmuller, Efficiency of ab-initio total energy calculations for metals and semiconductors using a plane-wave basis set, Comput. Mater. Sci. 6 (1996) 15–50.
[30] G. Kresse, J. Furthmueller, Efficient iterative schemes for ab initio total-energy calculations using a plane-wave basis set, Phys. Rev. B: Condens. Matter 54 (1996) 11169–11186.
[31] J.P. Perdew, K. Burke, M. Ernzerhof, Generalized gradient approximation made simple, Phys. Rev. Lett. 77 (1996) 3865–3868.
[32] H.J. Monkhorst, J.D. Pack, Special points for Brillouin-zone integrations, Phys. Rev. B 13 (1976) 5188–5192.
[33] A.T. Dinsdale, SGTE data for pure elements, CALPHAD: Comput. Coupling Phase Diagrams Thermochem. 15 (1991) 317–425.
[34] O. Redlich, A.T. Kister, Algebraic representation of thermodynamic properties and the classification of solutions, Ind. Eng. Chem. 40 (1948) 345–348.
[35] G. Kaptay, On the abilities and limitations of the linear, exponential and combined models to describe the temperature dependence of the excess Gibbs energy of solutions, Calphad 44 (2014) 81–94.
[36] G. Kaptay, On the tendency of solutions to tend toward ideal solutions at high temperatures, Metall. Mat. Trans. A 43 (2012) 531–543.
[37] M. Hillert, M. Jarl, A model for alloying effects in ferromagnetic metals, CALPHAD: Comput. Coupling Phase Diagrams Thermochem. 2 (1978) 227–238.
[38] G. Inden, Proceedings Project Meeting, Calphad V, Max-Planck Institute for Metal Research, Dusseldorf, 1976, pp. 1–13.
[39] C. Wagner, Thermodynamics of Alloys, Addison-Wesley Press, The University of California, 1952.
[40] E.R.M. Van, K.H.J. Buschow, Hydrogen absorption in various zirconium- and hafnium-based intermetallic compounds, J. Less-Common Met. 64 (1979) 277–284.
[41] H.L. Lukas, S.G. Fries, B. Sundman, Computational Thermodynamics: The CALPHAD Method, Cambridge University Press, 2007.
[42] P.A. Korzhavyi, I.A. Abrikosov, B. Johansson, A.V. Ruban, H.L. Skriver, First-principles calculations of the vacancy formation energy in transition and noble metals, Phys. Rev. B 59 (1999) 11693–11703.
[43] B. Sundman, B. Jansson, J.O. Andersson, The thermo-calc databank system, CALPHAD: Comput. Coupling Phase Diagrams Thermochem. 9 (1985) 153–190.
[44] Y. Du, R. Schmid-Fetzer, H. Ohtani, Thermodynamic assessment of the V–N system, Z. Metallkd. 88 (1997) 545–556.
[45] H.S. Chen, Glassy metals, Rep. Prog. Phys. 43 (1980) 353–433 353 plates.
[46] R.B. Schwarz, P. Nash, D. Turnbull, The use of thermodynamic models in the prediction of the glass-forming range of binary alloys, J. Mater. Res. 2 (1987) 456–460.
[47] P. Nash, R.B. Schwarz, Calculation of the glass forming range in binary metallic systems using thermodynamic models, Acta Metall. 36 (1988) 3047–3053.